ENHANCED SURFACE SPRAY COOLING WITH EMBEDDED AND COMPOUND EXTENDED SURFACE STRUCTURES

Eric A. Silk†
Thermal Engineering Branch
NASA Goddard Space Flight Center
Greenbelt, MD, USA, 20771
Tel:(301) 286-5534 Fax:(301) 286-1704
Email: Eric.A.Silk@nasa.gov

Jungho Kim
Department of Mechanical Engineering
University of Maryland
College Park, MD, USA, 20742
Tel:(301) 405-5437 Fax:(301) 314-9477
Email: kimjh@umd.edu

Ken Kiger
Department of Mechanical Engineering
University of Maryland
College Park, MD, USA, 20742
Tel:(301) 405- 5245 Fax:(301) 314-9477
Email: kkiger@umd.edu

ABSTRACT

Experiments were conducted to study the effects of enhanced surface structures on heat flux using spray cooling. The surface enhancements consisted of embedded structures (dimples, pores, and tunnels) and compound extended surface enhancements (straight fins, cubic pin fins and dimples) machined on and within the top surface of copper heater blocks. Each copper block had a projected cross-sectional area of 2.0 cm^2. Measurements were also obtained on a heater block with a flat surface for baseline comparison purposes. A 2x2 nozzle array was used with PF-5060 as the working fluid. Thermal performance data was obtained under nominally degassed (chamber pressure of 41.4 kPa) and gassy conditions (chamber with N_2 gas at 101 kPa) with a bulk fluid temperature of 20.5°C. Results for both the nominally degassed and gassy cases show that the highest critical heat flux (CHF) was attained using straight fins and porous tunnels. For the nominally degassed case, both had a CHF of ≈ 142 W/cm^2 while for the gassy case their CHF values increased to 175 W/cm^2. This gave an enhancement relative to the nominally degassed flat surface case of ≈ 77% and 119% respectively.

KEY WORDS: Enhanced Surfaces, Spray Cooling, Heat Transfer, Dissolved Gasses

NOMENCLATURE

A	Area, cm^2
$H1$	primary structure height, mm
$H2$	secondary structure height, mm
L	distance between successive structures, mm
P	pressure, kPa
R_a	Surface Roughness, μm
T	temperature, °C
TC	thermocouple
$\dot{V}''$	volume flux, m^3/m^2-s
X	structure width, mm
$d1$	pore/dimple diameter, mm
$d2$	tunnel diameter, mm
e	error
k	conductivity, W/m-K
l	nozzle height above heater surface, mm
q''	heat flux per unit area, W/cm^2
u	heat flux uncertainty, W/cm^2
x	thermocouple distance, mm
$z1$	pore/dimple depth into structure, mm

Greek symbols

Γ	weighted volume flux for concentric ring, %
ξ	heat flux to area enhancement factor ratio, $(q''_{surf}/q''_{flat})/(A_{surf}/A_{flat})$

Subscripts

i	concentric ring
k	conductivity, W/m-K
l	liquid
max	maximum
$surf$	surface
T	temperature, °C
x	thermocouple distance, mm

† Corresponding Author

INTRODUCTION

A great deal of research has been conducted to gain a better understanding of the general phenomena and critical parameters associated with spray cooling heat transfer. A review of the literature shows that previous studies have parametrically examined the effect of secondary gas atomizers vs. pressure atomizers [1,2], mass flux of ejected fluid [3,4], spray velocity [5,6], surface impact velocity [5,7,8], surface roughness [1,6,9,10], ejected fluid temperature, chamber environmental conditions, and spray footprint optimization on the effective heat flux across the heater surface [11]. Other topics studied to date include the effect of surfactant addition [12,13], and secondary nucleation [1,14,15].

This work is a continuation of the enhanced surface studies by Silk et al. [16-18], with an emphasis on surface embedded structures and compound extended surfaces as the feature of the surface enhancements. The objective of the current work is to examine the effects of these geometries and their arrangement on heat flux when using spray cooling.

Most previous studies that have examined enhanced surfaces have done so primarily from the perspective of surface roughness. Sehmbey et al. [1] gives an overview of spray cooling and provides a comparison of its effectiveness when using liquid and secondary gas atomizers (air used as the secondary gas). Heat flux was measured and presented for both techniques. Both the heat flux and the convection coefficient were found to have comparable values for both atomizer types. The authors concluded that the most important parameters affecting heat transfer are the fluid properties, spray velocity and surface conditions. It was also found that the heat transfer coefficient increased with the use of smooth surfaces (R_a< 0.1 μm) for gas atomized sprays, while the opposite trend was observed for liquid atomized sprays.

Pais et al. [10] studied the effects of surface roughness on heat transfer when using spray cooling. The surface roughnesses studied were 22, 14 and 0.3 μm. The sprayed surface was copper with a projected area of 1 cm^2. An air-assist atomizing nozzle was used with deionized water as the working fluid. Tests were conducted at a nozzle height of 23 mm. Tests were run up to CHF for all surface roughness values. It was found that the 0.3 μm surface achieved the highest heat flux, with a peak heat flux of 1250 W/cm^2. Furthermore, the onset of nucleate boiling was experienced at lower superheat values. The authors attributed the heat transfer enhancement to early bubble departure from the surface and nucleate boiling. The authors also concluded that secondary nucleation has a primary role as a heat transfer mechanism only if the surface finish is smooth.

Much work has been performed on pool boiling using enhanced surfaces. Surface modifications previously investigated include the use of paints, porous structures, and structured surface geometries (macro, micro and submicron-scale). Each of these techniques has been shown to enhance heat transfer given certain application constraints.

Honda et al. [19] investigated FC-72 boiling on silicon chips with micro-pin-fins, submicron-scale roughness and a combination surface utilizing both enhancements. The square pins had dimensions of 50 x 50 x 60 μm^3, while the submicron-scale roughened surface had a Root Mean Square (RMS) roughness between 25-32 nm. The effects of subcooling and dissolved gasses on heat flux were reported for each of these surfaces. The submicron-scale roughened surface displayed a higher heat transfer than the micro-pin-finned surface at low heat flux values. The opposite trend was observed at high heat flux. The combination surface displayed the highest heat transfer of all the surfaces with a CHF value of 1.8 to 2.3 times larger than the corresponding smooth surface case. CHF was found to vary linearly with subcooling for all chips.

Chien and Webb [20] investigated the effects of structured tunnel dimensions on nucleate boiling convection coefficients for heat fluxes ranging between 2 and 70 kW/m^2. Tests were performed on a 19.1 mm diameter horizontal tube using R-11 and R-123 as working fluids. Tunnel pitch, height, width, and base radius were the primary dimensions studied. The authors found that fins shorter than 0.9 mm experienced significant increases in the convection coefficient as the fin count increased from 1378 fins/m to 1575 fins/m. They also found that using straight fins promoted increased evaporation by retaining more liquid between neighboring fins. Increased fin height had little effect on the convection coefficient. Fin pitch was also observed to have little effect.

The initial work by Silk et al. [16] showed that spray cooling of enhanced surface structures such as cubic pin fins, straight fins, and pyramids results in a corresponding heat flux enhancement. The present work extends the initial investigation to include embedded structures and compound extended surface enhancements. Spray cooling heat flux as a function of geometry and structure arrangement is reported. Six new geometries were tested for heat flux comparison between one another as well as comparison to geometries tested in previous studies [16] (i.e. cubic pin fins and straight fins). The new surfaces tested include thin straight fins (1s_t), straight fins with cubic pin fins on top (1sc), surface dimples (1d), straight fins with surface dimples in the fins and on the base (1sd), radial fins (1r), and porous tunnels (1pt). It was found that CHF for the thin straight fin and porous tunnel surfaces was nearly the same in the degassed (≈ 142 W/cm^2) and gassy (≈ 175 W/cm^2) cases. Furthermore, each of these outperformed the other surfaces.

TEST SETUP AND PROCEDURE

The experiments were conducted using a closed fluid loop system. The test rig (schematic shown in Fig. 1) consisted of an environmental test chamber, liquid pump, flow meter, micro-filter and a condenser. Chamber temperature and pressure were measured via a T-type thermocouple and a pressure sensor. Temperature and pressure sensors were also placed in the liquid line upstream of the nozzle for fluid and supply line temperature and pressure measurement.

Each of the test heaters were made of oxygen free copper with a uniform undercoat of 2.54 μm nickel and 1.27 μm top-surface coat of gold. Heat was supplied to the test article using a 500 W cartridge heater. The test article was placed within the interior of the chamber, but was separated from the excess liquid by an enclosure consisting of a polycarbonate housing and an alumina bisque ceramic top flange (Fig. 2).

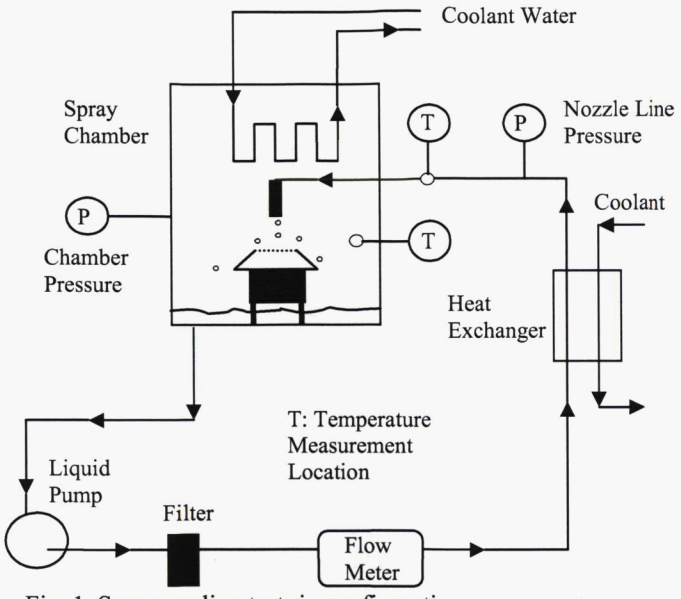

Fig. 1 Spray cooling test rig configuration

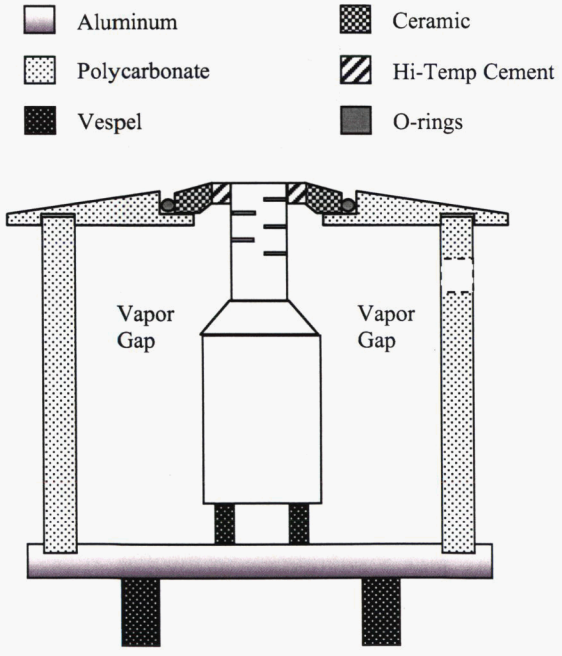

Fig. 2 Copper block housing schematic

The upper section of the copper block was epoxied to the ceramic flange. Temperature measurements in the copper blocks were sampled via five T-type thermocouples mounted in the upper section of each block (Fig. 3). Assuming steady state 1-D conduction through the upper portion of the block, the heat flux was calculated using Fourier's Law. The reported heat flux was determined as the average values from multiple pairs of thermocouples (TC1 through TC5). Surface temperature was determined via linear extrapolation using TC1 and TC2.

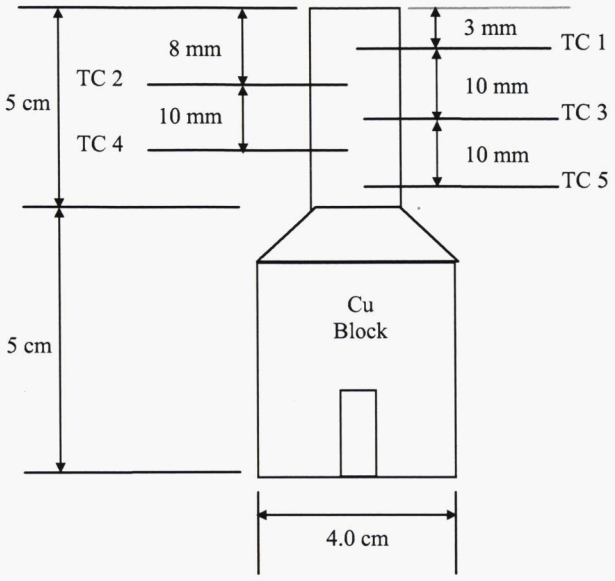

Fig. 3 Copper block schematic with TC locations (not to scale)

Table 1. Test case conditions

Spray Cooling Parameters		
Parameters	Degassed Case	Gassy Case
P_{sat}	41.4 kPa	101 kPa
T_{sat}	31 °C	56 °C
T_l	20.5 °C	20.5 °C
h_{fg}	92 kJ/kg	76 kJ/kg
Gas Content	470 ppm	3821 ppm

Prior to each test, the spray chamber and fluid loop were charged with PF-5060. A vacuum was repeatedly applied to the chamber until a pressure of 41.4 kPa (470 ppm gas concentration) was reached. For the gassy case, the chamber was backfilled to 101 kPa using N_2 gas (99.9% purity). The gas concentration for this case was 3821 ppm. The chamber was allowed to attain equilibrium prior to conducting the tests. Test conditions for both the gassy and degassed cases are shown in Table 1.

All tests were run at constant chamber pressure, liquid flow rate (200 ml/min) and constant nozzle height above the heater surface. Heat was supplied to the cartridge heater in increments of 10 W using a programmable power supply. Steady state was achieved at each power level, and data was acquired before application of the next successive heat load. Upon dry-out (detected by a rapid increase in surface temperature and a rapid decrease in heat flux), power to the cartridge heater was turned off.

A Parker Hannifin prototype spray nozzle consisting of a 2x2 spray cone array was used for each of the tests. Prior to heat flux testing, the spray nozzle uniformity was measured using stainless steel tubes of varying inner diameters, a graduated cylinder, and a stopwatch. The largest tube had an

Section	Area (cm^2)	Area (%)	Vol. Flux (m^3/m^2 s)	Γ_i
A_1	0.33	17.5	0.026	2.0
A_2	0.38	20	0.024	1.8
A_3	0.54	28.5	0.007	0.6
A_4	0.64	34	0.005	0.4

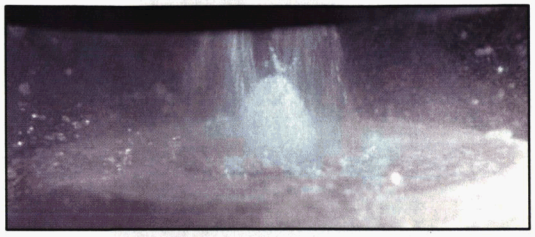

In-situ photo of center-weighted spray on flat surface

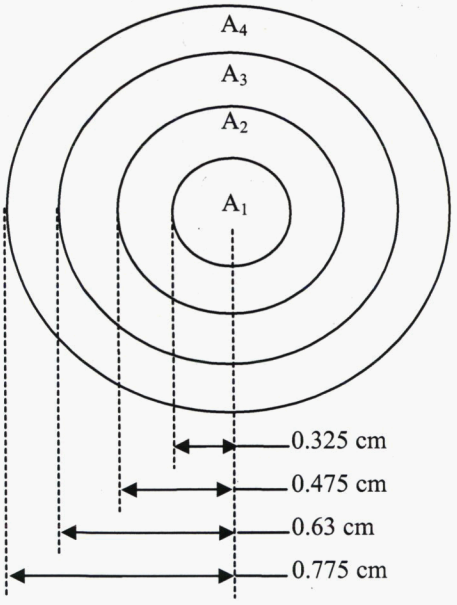

Fig. 4 Spray uniformity test schematic (not to scale)

inner diameter approximately the same diameter as the heated surface. Size, local volume flux between concentric cylinders, and the local volume flux between concentric cylinders normalized by the average volume flux over the entire heater surface (Γ) are shown in Fig. 4. A Γ value of unity indicates that the local volume flux is identical to the total volume flux averaged across the entire heater surface. The outer ring (A_4) captured 60% less volume flux than the average area value.

The volume flux gradually increased towards the center of the heater region. The center ring (A_1) had twice as much volume flux as the average for the entire area. Given the volume flux variation throughout the concentric rings, the spray could be considered a non-uniform center biased spray for the current nozzle height and heater area. Spray characteristics were not investigated during this study.

The feature geometry dimensions of each surface are summarized in Table 2. Schematics and photographs of the enhanced surfaces are shown in Fig. 5. The cross-sectional view shown for the radial fin surface (1r) highlights channel dimensions. These channels were positioned on the top of the surface every 15°. The axes shown in the porous tunnel surface (1pt) picture are for reference regarding the subsurface structure geometry. The tunnels were uni-directional along the x axis (i.e. extended along a constant y value). The centerline of each tunnel was aligned with the centerline of a row of pores drilled normal to the surface. Each tunnel extended through the entire cross section of the copper block. The perimeter of that cross section (including the areas immediately circumscribing the perimeter of the tunnel outlets) was insulated with epoxy. This limited liquid contact to the top surface, the pore interior, and the interior of the tunnels.

Table 2. Enhanced surface geometry summary

Surface	Dimensions in (mm)						
	X	L	H1	H2	d1	d2	z1
Flat Surface (1f)	0	0	0	--	--	--	--
Straight Fins (1s)	1.0	1.0	1.0	--	--	--	--
Cubic Pin Fins (1c)	1.0	1.0	1.0	--	--	--	--
Thin Straight Fins (1s_t)	0.5	0.5	1.0	--	--	--	--
Straight fins w/Cubics (1sc)	1.0	1.0	0.5	0.5	--	--	--
Dimples (1d)	--	1.0	--	--	0.5	--	0.5
Straight Fins w/Dimples (1sd)	1.0	1.0	1.0	--	0.5	--	0.5
Radial Fins (1r)	--	0.5	1.0	--	--	--	--
Porous Tunnels (1pt)	--	--	--	--	1.0	1.0	0.5

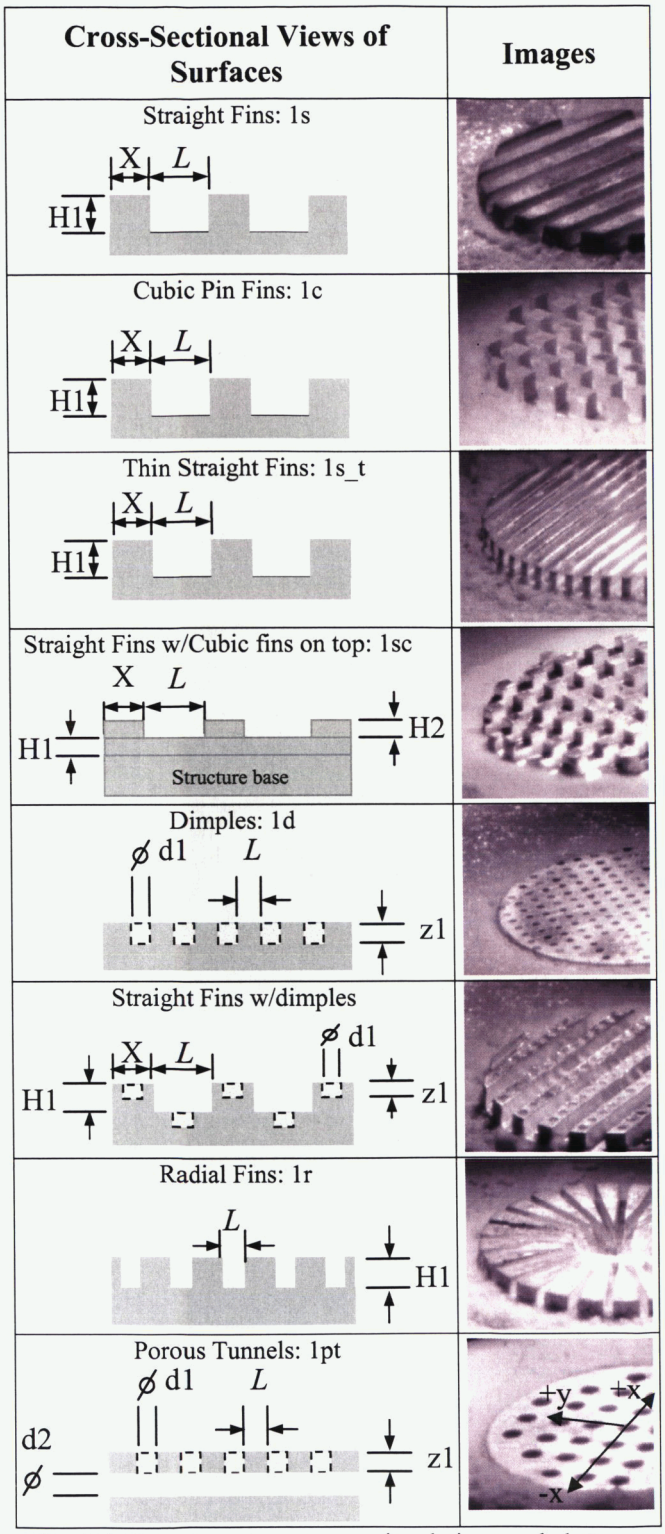

Fig. 5 Surface geometry cross sectional views and photos

MEASUREMENT UNCERTAINTY

The primary quantity of interest for these experiments is the heat flux. The heat flux calculation has three primary contributions to the uncertainty: the conductivity, the thermocouple locations, and the error in the temperature measured. The conductivity value used was 389 W/m K with 1% error. The error in the thermocouple temperature measurements was estimated as ±0.5°C. The error in the thermocouple location was determined to be ±0.56 mm. Equation 1 was used to calculate the error for the heat flux values reported. The uncertainty in the heat flux was determined to be 5.6% at 80 W/cm^2. Calculations indicated that heat losses within the upper neck of the copper block were less than 1% of the total heat input at CHF for the flat surface case. Spray cooling heat flux demonstrated a repeatability within 1% for multiple tests under identical test conditions. Pressure values had an uncertainty of ±3 kPa. Flow meter measurements had an error of ±1 ml/min.

$$u_{q''} = \pm \sqrt{\sum_{j=1}^{N} \frac{\left[\left(\frac{\partial q''_j}{\partial x} e_x\right)^2 + \left(\frac{\partial q''_j}{\partial k} e_k\right)^2 + \left(\frac{\partial q''_j}{\partial (\Delta T)} e_{\Delta T}\right)^2\right]}{N^2}} \quad (1)$$

RESULTS AND DISCUSSION

Heat flux performance as a function of the structure geometry for each of the surfaces is shown in Figs. 6, 7 and 8. for the nominally degassed cases. Comprehensive heat flux results for the gassy case are shown in Fig. 10. The calculated heat flux is based on the projected area (2.0 cm^2) for all cases (not the wetted surface area exposed to the fluid).

Embedded Structures (Dimpled and Porous Structures)

Fig. 6 shows heat flux as a function of surface temperature and embedded structure geometry under nominally degassed conditions. The heat transfer variation for all surfaces is linear in the low heat flux regime, which is indicative of single phase convection. Multiphase effects become pronounced (denoted by the increase in slope of the heat flux curves) around $T_{surf} \approx 50°C$ for the porous tunnel (1pt) surface. For the flat (1f) and dimpled surfaces (1d), multiphase effects do not become pronounced until $T_{surf} \approx 55°C$. Both of the embedded structures had a significant increase in CHF relative to the flat surface case thus indicating heat flux enhancement may be attained with spray cooling using both extended and embedded structure geometries. The porous tunnels (1pt) had the highest CHF (140 W/cm^2) of the surfaces tested in this case.

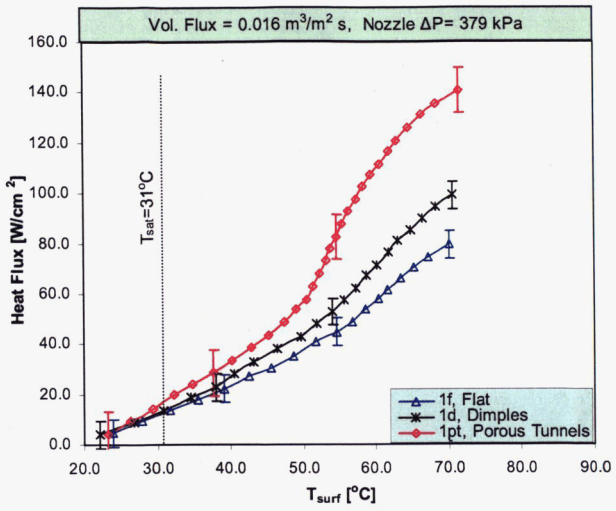

Fig. 6. Heat flux as a function of surface temperature for embedded structure geometries

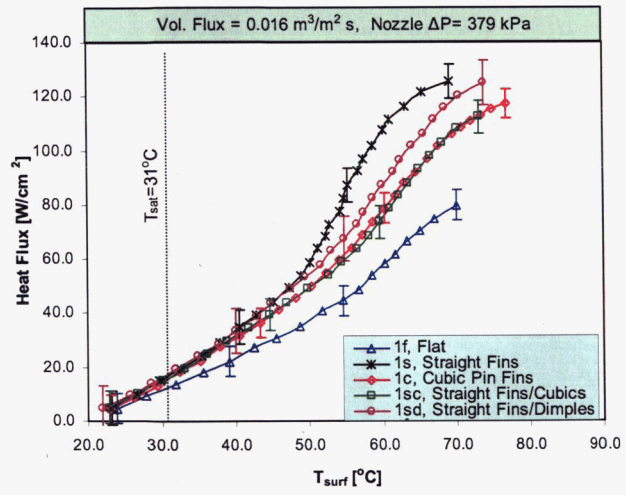

Fig. 7. Heat flux as a function of surface temperature for straight and cubic pin fin geometries.

Straight Fins vs. Cubic Pin Fins

Fig. 7 shows heat flux as a function of surface temperature and extended surface fin geometry under nominally degassed conditions. The straight and cubic pin fin data, previously reported in Silk et al. [16], is also reported here for comparison with the straight fin surfaces with cubic pin fins and with dimples (i.e. surfaces 1sc and 1sd). Heat transfer variation for all surfaces is linear in the low heat flux regime. Multiphase effects become observable around $T_{surf} \approx$ 40°C and pronounced around $T_{surf} \approx$ 48°C for surface 1s. In the multiphase regime, the spray cooling curves for surfaces 1s and 1sd separate and show surface 1s performing noticeably better (beyond the range of experimental uncertainty) than surface 1sd. However, each of these surfaces approach the same nominal CHF value in the high heat flux regime. Surfaces 1c and 1sc have nearly identical (well within the experimental uncertainty) heat flux performance throughout the low heat flux, multiphase, and high heat flux regimes. Both transition to the multiphase regime around $T_{surf} \approx$ 52°C. The highest CHF was attained with the straight fin and straight fin w/dimples surfaces (126 W/cm^2 and 125 W/cm^2 respectively). Surfaces 1c and 1sc attained CHF values of 117 W/cm^2 and 112 W/cm^2 respectively.

The results of the initial enhanced surface spray cooling study by Silk et al. [16] were non-intuitive. It was clearly shown (and is shown here as well), that the straight fin (1s) surface had better heat flux performance than the cubic pin fin (1c) surface even though the area increase relative to the flat surface (2.0 cm^2) was the same (the total area exposed to the liquid for both surfaces was 4.0 cm^2). The implication from these results was that liquid management on the 1s surface promoted better heat transfer than the 1c surface.

Further investigation into the differences in heat flux performance between the two geometries (1s and 1c) must incorporate a discussion of the effective area utilized. This can be investigated using one of two methodologies. The first is through visualization. However, this is problematic since the large spray density obscures the surface. The second is through heat flux testing using surfaces specially designed to provide more insight into heat flux performance as a function of geometry. The second was employed in this investigation in the form of surface 1sc.

The difference in structure geometry between surface 1s and 1c is the cutaway volumes (cubes) prevalent on the 1c surface. The surface area on the top of the fins in the 1s case is transplanted to the base of the structure when volumetric sections are removed from the straight fins to create cubic pin fins. Surface 1sc is a special geometry which is a hybrid between the two surfaces. Surface 1sc has continuous sidewall area at the base of the structure (similar to the straight fins) up to a height of 0.5 mm. Above that height, surface 1sc is similar to surface 1c. The heat flux data in Fig. 7 shows that surface 1sc performs similarly to surface 1c. This implies that the heat flux enhancement observed with surface 1s is due to heat transfer along the upper sidewall area of the straight fins (i.e. 0.5 mm < H ≤ 1.0 mm) and the top of the fin surfaces. We can conclude that the larger enhancement in the straight fins is due to more upper sidewall and top surface area.

Radial vs. Straight Fins

Fig. 8 shows heat flux as a function of surface temperature and straight fin geometry under nominally degassed conditions. Multiphase effects become pronounced for each of the enhanced surfaces around $T_{surf} \approx$ 50°C. However, the thin straight fin surface (1s_t) has a much more linear progression to CHF than both the radial fins (surface 1r) and the straight fins (surface 1s). Surfaces 1s and 1r show fair agreement in the multiphase regime until $T_{surf} \approx$ 60°C, at which point they both transition to the high heat flux regime. The highest CHF (144 W/cm^2) was attained with surface 1s_t. Surface 1r had a CHF of 136 W/cm^2 and surface 1s (as previously reported in Ref. 16) had a CHF of 126 W/cm^2.

Investigation of spray cooled radial fins presents a different fin approach and geometry in comparison to previously investigated structures [16-18]. The 2x2 Parker Hannifin spray manifold used for these studies creates a stag-

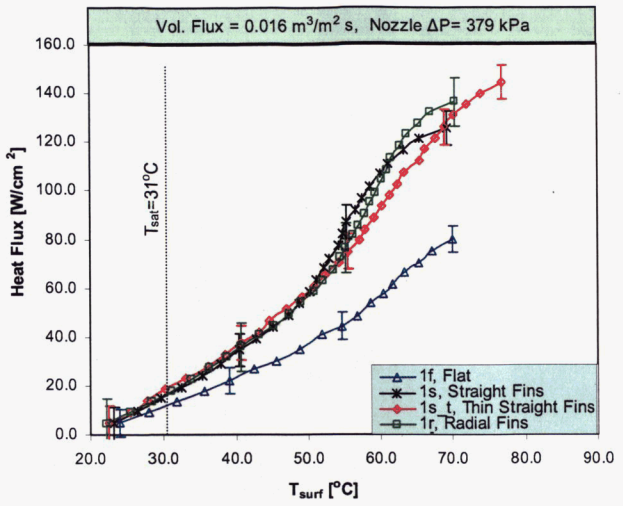

Fig. 8. Heat flux as a function of surface temperature for straight and radial fin geometries

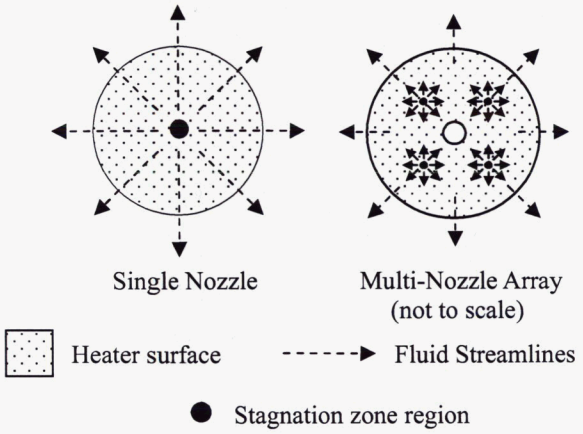

Fig. 9. Plan view of flat heater surface liquid flows

nation zone in the center of the heat exchange surface [18]. Droplets that do not rebound off of the surface become entrained in the liquid flow on the heater surface. This flow moves outward radially from the stagnation zone as it is convected from the heater surface (see Fig. 9). Structures tested prior to this study (including many structures in this study) have been based on Cartesian coordinates. However, the flow across the surface (outside of the stagnation zone) is in the radial direction. The usage of Cartesian based fin arrangements with a radial flow essentially creates a scenario where the fins are mis-aligned with the surface flow. Thus, spray cooling with radial fins may be considered aligned fin spray cooling.

The difference between the extended surface enhanced structures and the flat surface is the fin side wall area. The nominal area addition between any extended structure and the flat surface may be attributed to the sidewall area. The channels created by the extended structures (and their respective geometries) are of importance regarding the total area available and aid in determining the mechanisms of heat transfer enhancement for these structures. Surfaces 1s_t and 1r are similar in that they have the same channel aspect ratio X/H = 0.5 mm/1.0 mm. However, the total surface areas are different due to differences in the channel length and the number of channels in the radial case. While the nominal heat flux values are greater for 1s_t, the heat flux to area enhancement factor ratio is only 0.6 whereas for the 1r surface it is 0.74 (degassed case). For the gassy case the ξ values decrease to 0.53 and 0.69 respectively. This implies that radial fins are more efficient for the given spray nozzle used.

Case 1s_t was created by reducing the previously used fin width and separation distance for case 1s by a factor of two. In comparison to surface 1s, surface 1s_t has twice the sidewall area addition (4.0 cm^2) and twice the fin count while maintaining the same total surface area for the top of the fins and the same total base area between fins. Thus area addition relative to surface 1s is through the fin sidewalls. The nominal increase in heat flux between surfaces 1s and 1s_t shows diminishing returns with the addition of sidewall area. A comprehensive summary of the degassed data including the total wetted surface area (A_{surf}), CHF, corresponding surface temperature at CHF, and heat flux to area enhancement factor ratio (relative to the flat surface case) is shown in Table 3.

Table 3. Summary of Degassed case Enhanced Surface data

Surface	A_{surf} (cm^2)	q''_{CHF} (W/cm^2)	T_{max} (°C)	Heat Flux/Area Enhancement factor $\xi_{degassed}$
‡1f	2.0	80	70	1.0
‡1s	4.0	126	69.1	0.79
‡1c	4.0	117	76.8	0.73
1sc	4.0	112	73.1	0.7
1sd	5.2	125	73.8	0.6
1s_t	6.0	144	76.9	0.6
1r	4.6	136	70.2	0.74
1d	3.2	99	70.6	0.77
1pt	7.5	140	71.4	0.47

‡ denotes data previously published by Silk et al. [16]

Dissolved Gas Study

Dissolved gas spray cooling with enhanced surfaces has been shown to provide additional enhancement to heat flux [16,17]. Spray cooling performance with dissolved gasses for each of the new geometries presented in this study are shown in Figure 10. The porous tunnel (1pt) and radial fin (1r) surfaces were the first to transition into the multiphase regime around $T_{surf} \approx 65°C$. The thin straight fins (1s_t) and straight fins with dimples (1sd) surfaces showed pronounced multiphase effects around $T_{surf} \approx 70°C$. The straight fins with cubics (1sc), dimples (1d), and flat surfaces (1f) each transitioned to the multiphase regime around $T_{surf} \approx 75°C$. The radial fins (1r) and porous tunnels (1pt) agreed well throughout each of the heat flux regimes. The thin straight fins (1s_t) and the straight fins with dimples (1sd) agreed well before their transition into the high heat flux regime at $T_{surf} \approx$ 83°C. The dimples (1d) and the straight fins with cubics (1sd) agreed well within the multiphase regime only to diverge

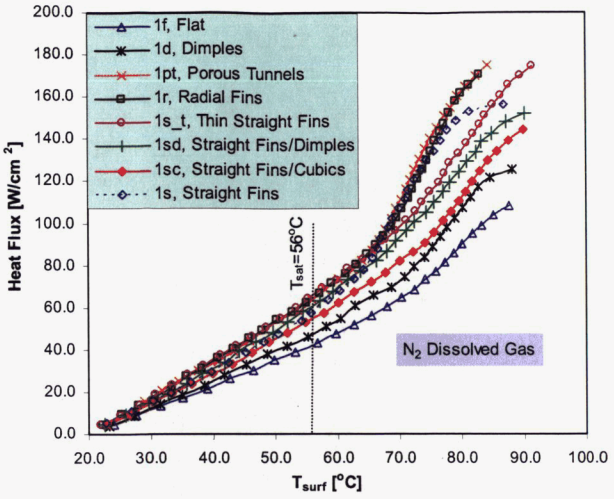

Fig. 10. Heat flux as a function of surface temperature and geometry with N_2 dissolved gasses

Table 4. Summary of Gassy case Enhanced Surface data

Surface	A_{surf} (cm^2)	q''_{CHF} (W/cm^2)	T_{max} (°C)	Heat Flux/Area Enhancement factor ξ_{gassy}
‡1f	2.0	108	87.5	1.0
‡1s	4.0	156	86.7	0.72
‡1c	4.0	145	93.3	0.67
1sc	4.0	145	89.9	0.67
1sd	5.2	153	90.2	0.54
1s_t	6.0	175	91.5	0.53
1r	4.6	171	82.9	0.69
1d	3.2	126	88.3	0.73
1pt	7.5	175	84.2	0.43

‡ denotes data previously published by Silk et al. [16]

when transitioning to the high heat flux regime. The straight fins with dimples (1sd) and the straight fins with cubics (1sc) converged as they approached CHF. The porous tunnels (1pt) and the thin straight fins (1s_t) both attained a CHF of 175 W/cm^2. This was the highest CHF attained by any of the surfaces in the gassy case. The radial fins (1r) had the second highest CHF of 171 W/cm^2 which is within the experimental uncertainty of the data collected. Table 4 gives a summary of the total wetted surface area (A_{surf}), CHF, corresponding surface temperature at CHF, and heat flux to area enhancement factor ratio.

The dissolved gasses delayed the transition between the low, intermediate and high heat flux regimes. This allowed for higher surface temperatures to be attained prior to dry-out. Lin and Ponnappan [21] concluded that noncondensible gasses enhanced heat transfer due to increased film spreading initiated by a reduction in the partial vapor pressure within the liquid film vicinity. Horacek et al. [22] determined that the delay in transition between heat flux regimes when performing dissolved gas spray cooling was due to the working fluid effectively being subcooled by the gas.

CONCLUSIONS

Spray cooling heat flux measurements were performed on extended and embedded enhanced surfaces as well as a flat surface using PF-5060. Tests were performed under nominally degassed (fluid at 41.4 kPa) and gassy (N_2 dissolved gas at 101 kPa) conditions. The volumetric flow rate (0.016 m^3/m^2s) and nozzle height from the surface (17 mm) were held constant for all the tests.

The porous tunnels attained the highest CHF for the embedded structures tested under both nominally degassed (140 W/cm^2) and gassy conditions (175 W/cm^2).

The straight fins with cubics surface (1sc) had nearly identical heat flux performance with the cubic pin fin surface (1c). It was concluded that surface 1s attained higher heat fluxes compared to 1c due to additional upper sidewall area and the fin top area available for heat exchange.

The thin straight fin surface (1s_t) had the highest CHF (144 W/cm^2) for the straight vs. radial fin study in the degassed case. For the gassy case the CHF value increased to 175 W/cm^2, however surface 1r had a CHF of 171 W/cm^2 which is well within the experimental uncertainty.

The radial fin surface (1r) had a higher ξ value compared to the thin straight fins for both the degassed and gassy cases.

Surfaces 1s_t and 1pt attained the highest CHF values for the gassy case study. Each of these were 175 W/cm^2.

ACKNOWLEDGMENTS

This research was supported by the Thermal Management group of the Laboratory for Physical Sciences and funded by the Laser Risk Reduction Program (LRRP) at the NASA Goddard Space Flight Center. Dr. Jungho Kim and Dr. Kenneth Kiger would like to acknowledge the generous support of the Office of Naval Research under contract number N000140410315 directed by Dr. Mark Spector. The authors would like to thank Dr. Paul Boudreaux, for his assistance, as well as J.B. Dotellis and Lester Lorentz for their support in machining the copper test articles and their surfaces. Special thanks is also given to Richard Freburger and Alice Rector of NASA Goddard Space Flight Center, Juan Rodriguez of University of Puerto Rico at Mayaguez for their test support as well as Parker Hannifin's Gas Turbine Fluid Systems Division (GTFSD) for supplying the spray nozzle.

REFERENCES

[1] Sehmbey, M., Chow, L., Pais, M., and Mahefkey, T., 1995, "High heat flux spray cooling of electronics," *12th Symposium on Space Nuclear Power and propulsion*, Albuquerque, NM, Jan., AIP Conference Proceedings no. 324, pp. 903-909

[2] Yang, J., Pais, M., and Chow, L., 1993, " Critical Heat Flux Limits In Secondary Gas Atomized Liquid Spray Cooling," *Experimental Heat Transfer,* Vol. 6, pp. 55-67

[3] Estes, K.A., and Mudawar, I., 1995, "Correlation of Sauter mean diameter and critical heat flux for spray cooling of small

surfaces," *International Journal of Heat and Mass Transfer,* Vol.38, No.16, pp. 2985-2996

[4] Yang, J., Chow, L., and Pais, M., 1996, "Nucleate Boiling Heat Transfer in Spray Cooling," *Journal of Heat Transfer*, Vol. 118, pp. 668-671

[5] Chen, R-H., Chow, L., and Navedo, J., 2002, "Effects of spray characteristics on critical heat flux in subcooled water spray cooling," *International Journal of Heat and Mass Transfer*, Vol. 45, pp. 4033-4043

[6] Sehmbey, M., Pais, M., and Chow, L., 1992, "A study of diamond laminated surfaces in evaporative spray cooling," *Thin Solid Films*, Vol. 212, pp. 25-29

[7] Healy, W., Halvorson, P., Hartley, J., and Abdel-Khalik, S., 1998, "A critical heat flux correlation for droplet impact cooling at low Weber numbers and various ambient pressures," *International Journal of Heat and Mass Transfer*, Vol. 41, pp. 975-978

[8] Sawyer, M., Jeter, S., and Abdel-Khalik, S., 1997, "A critical heat flux correlation for droplet impact cooling," *International Journal of Heat Transfer*, Vol. 40, No. 9, pp.2123-2131

[9] Bernadin, J.D., and Mudawar, I., 1999, "The Leidenfrost Point: Experimental Study and Asessment of Existing Models," *Journal of Heat Transfer*, Vol. 121, pp. 894-903

[10] Pais, M., Chow, L., and Mahefkey, E., 1992, " Surface Roughness and Its Effects on the Heat Transfer Mechanism of Spray Cooling," *Journal of Heat Transfer*, Vol. 114, No. 1, pp. 211-219

[11] Mudawar, I., and Estes, K., 1996, "Optimizing and Predicting CHF in Spray Cooling of a square surface," *Journal of Heat Transfer*, Vol. 118, pp. 672-679

[12] Qiao, Y.M., and Chandra, S., 1997, " Experiments on adding a surfactant to water drops boiling on a hot surface," *Proceedings of the Royal Society of London*, Vol. 453, pp. 673-689

[13] Qiao, Y., and Chandra, S., 1998, "Spray Cooling Enhancement by Addition of a Surfactant," *Journal of Heat Transfer*, Vol. 120, pp. 92-98

[14] Mesler, R., 1993, " Surface Roughness and It's Effects on the Heat Transfer Mechanism of Spray Cooling," *Journal of Heat Transfer*, Vol. 115, pp. 1083-1085

[15] Rini, D., Chen, R.-H., Chow, L., 2002, "Bubble Behavior and Nucleate Boiling Heat Transfer in Saturated FC-72 Spray Cooling," *Journal of Heat Transfer*, Vol. 124, pp. 63-72

[16] Silk, E.A., Kim, J., and Kiger, K., 2004, "Investigation of Enhanced Surface Spray Cooling," *ASME International Mechanical Engineering Congress,* Anaheim, CA, Nov.13-19, IMECE2004 Conference Proceedings

[17] Silk, E.A., Kim, J., and Kiger, K., 2005, "Impact of Cubic Pin Finned Surface Structure Geometry Upon Spray Cooling Heat Transfer," *ASME International Electronic Packaging and Technical Conference,* San Francisco, CA, July. 17-22, InterPACK 2005 Conference Proceedings

[18] Silk, E.A., Kim, J., and Kiger, K., 2005, "Spray Cooling Trajectory Angle Impact Upon Heat Flux Using a Straight Finned Enhanced Surface," *ASME 2005 Heat Transfer Summer Conference,* San Francisco, CA, July .17-22, HT2005 Conference Proceedings

[19] Honda, H., Takamastu, H., and Wei, J.J., 2002, "Enhanced Boiling of FC-72 on Silicon Chips With Micro-Pin-Fins and Submicron-Scale Roughness," *Journal of Heat Transfer*, Vol. 124, pp. 383-390

[20] Chien, L.H., and Webb, R.L., 1998a, "A Parametric Study of Nucleate Boiling on Structured Surfaces, Part I: Effect of Tunnel Dimensions," *Journal of Heat Transfer*, Vol. 120, pp. 1042-1048

[21] Lin, L., and Ponnappan, R., 2003, " Heat Transfer Characteristics of Evaporative Spray Cooling in a Closed Loop," *International Journal of Heat Transfer*, Vol. 46, pp. 3737- 3746

[22] Horacek, B., Kiger, K., Kim, J., "Single Nozzle Spray Cooling Heat Transfer Mechanisms", *International Journal of Heat and Mass Transfer*, Vol. 48, No. 8, pp. 1425-1438, 2005